



**HAL**  
open science

# Elastic Vector Solitons in Soft Architected Materials

Bolei Deng, J. R. Raney, Vincent Tournat, K. Bertoldi

► **To cite this version:**

Bolei Deng, J. R. Raney, Vincent Tournat, K. Bertoldi. Elastic Vector Solitons in Soft Architected Materials. *Physical Review Letters*, 2017, 118 (20), pp.204102. 10.1103/PhysRevLett.118.204102 . hal-01703881

**HAL Id: hal-01703881**

**<https://univ-lemans.hal.science/hal-01703881>**

Submitted on 8 Feb 2018

**HAL** is a multi-disciplinary open access archive for the deposit and dissemination of scientific research documents, whether they are published or not. The documents may come from teaching and research institutions in France or abroad, or from public or private research centers.

L'archive ouverte pluridisciplinaire **HAL**, est destinée au dépôt et à la diffusion de documents scientifiques de niveau recherche, publiés ou non, émanant des établissements d'enseignement et de recherche français ou étrangers, des laboratoires publics ou privés.



## Elastic Vector Solitons in Soft Architected Materials

B. Deng,<sup>1</sup> J. R. Raney,<sup>2</sup> V. Tournat,<sup>1,3</sup> and K. Bertoldi<sup>1,4</sup>

<sup>1</sup>*Harvard John A. Paulson School of Engineering and Applied Sciences, Harvard University, Cambridge, Massachusetts 02138, USA*

<sup>2</sup>*Department of Mechanical Engineering and Applied Mechanics, University of Pennsylvania, Philadelphia, Pennsylvania 19104, USA*

<sup>3</sup>*LAUM, CNRS, Université du Maine, Avenue Olivier Messiaen, 72085 Le Mans, France*

<sup>4</sup>*Kavli Institute, Harvard University, Cambridge, Massachusetts 02138, USA*

(Received 9 February 2017; published 17 May 2017)

We demonstrate experimentally, numerically, and analytically that soft architected materials can support the propagation of elastic vector solitons. More specifically, we focus on structures comprising a network of squares connected by thin and highly deformable ligaments and investigate the propagation of planar nonlinear elastic waves. We find that for sufficiently large amplitudes two components—one translational and one rotational—are coupled together and copropagate without dispersion. Our results not only show that soft architected materials offer a new and rich platform to study the propagation of nonlinear waves, but also open avenues for the design of a new generation of smart systems that take advantage of nonlinearities to control and manipulate the propagation of large amplitude vibrations.

DOI: [10.1103/PhysRevLett.118.204102](https://doi.org/10.1103/PhysRevLett.118.204102)

Highly deformable, soft structures characterized by a nonlinear response have enabled the design of new classes of tunable and responsive systems and devices, including soft robots [1,2], self-regulating microfluidics [3], reusable energy absorbing systems [4,5], and materials with programmable response [6]. Furthermore, soft architected materials (also referred to as soft or nonlinear metamaterials) present opportunities to control the propagation of elastic waves, since their dispersion properties can be altered by applying a large, nonlinear predeformation [7–9]. However, most of the investigations have exclusively focused on linear stress waves, although the compliant nature of soft systems is capable of supporting large-amplitude nonlinear waves.

Nonlinear waves not only display a very rich behavior, but also enable a broad range of applications, including impact mitigation layers [10,11], asymmetric transmission [12,13], switches [14], and lenses [15]. While such waves have mostly been studied in granular media [10–16], soft architected materials also provide an ideal environment for their propagation. In fact, even soft metamaterials made of a single linear material can support a wide range of effective nonlinear behaviors that are determined by the architecture. This marks an important difference between soft architected materials and granular media, since in the latter the nonlinear response is determined by the contacts between grains, and those are difficult to control [17], especially in 2D.

In this Letter, we combine analytical, numerical, and experimental tools to study the propagation of large-amplitude nonlinear waves in a structure comprising a network of squares connected by thin and highly deformable ligaments. While the behavior of this system under quasistatic loading has attracted significant interest as it is characterized by an effective negative Poisson ratio

[18–20], here we focus on its dynamic response and demonstrate how the geometry of the system directly affects its nonlinear dynamic elastic properties. We investigate the propagation of nonlinear waves of mixed translational and rotational nature and demonstrate the existence of vector elastic solitons. Moreover, we show that by tuning the geometry of the structure a wide range of dispersive and nonlinear dynamic properties can be achieved.

Our system consists of a network of square domains connected by thin ligaments (see Fig. 1), all made of elastomeric material [polydimethylsiloxane (PDMS)]. The squares have edge lengths of approximately 8 mm and diagonals of length  $2l \approx 11.3$  mm that are rotated by an angle  $\theta_0 = 25^\circ$  with respect to the horizontal and vertical directions [see Fig. 1(a)]. A system comprising  $6 \times 40$  squares is fabricated with high fidelity using direct ink writing, an extrusion-based 3D printing method [21,22] [see Supplemental Material (SM) for details [23]]. After printing, all squares are filled with PDMS and a small copper cylinder with radius 2.38 mm is also placed at their center in order to modify the medium inertial properties.

We start by investigating experimentally the propagation of pulse waves in the system. Impact experiments are conducted in which a custom aluminum impactor is used to initiate simultaneous rotation and displacement of the squares at one end of the sample [see Fig. 1(a) and Movies S1 and S2 in SM [23]]. Different displacement signals are applied to the first column of square by varying both the initial gap between the impactor and the structure (defining the maximum imposed displacement) and the strength of the pulse applied to the impactor (mostly influencing the maximum imposed velocity). The propagation of the resulting pulses through the entire sample is

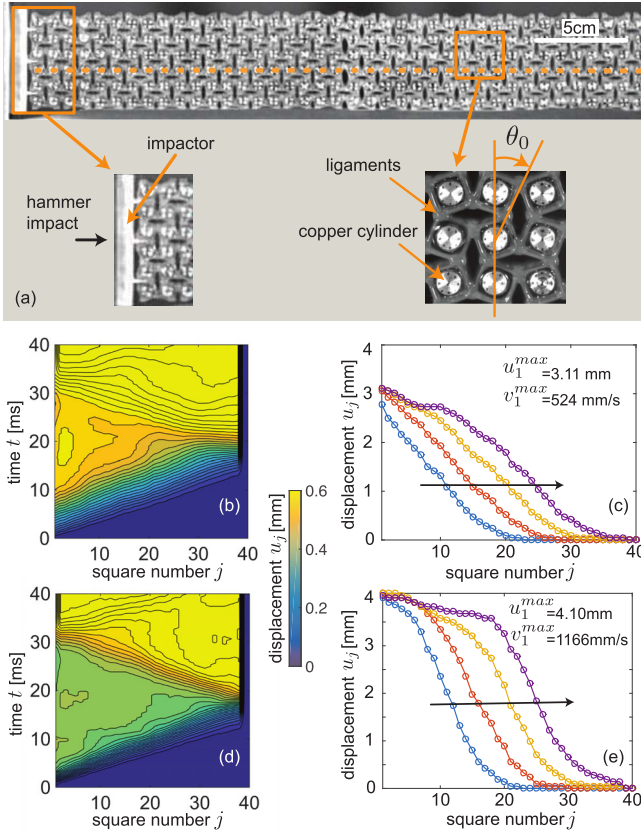


FIG. 1. (a) The system consists of a network of square domains connected by thin ligaments. Pulse waves are generated by a hammer strike on an aluminium impactor and propagate from left to right. (b)–(d) Spatiotemporal displacement diagrams and (c)–(e) spatial displacement profiles at  $t = 7, 10, 13, 16$  ms for an impact characterized by (b),(c)  $(u_1^{\max}, v_1^{\max}) = (3.11 \text{ mm}, 524 \text{ mm/s})$  and (d),(e)  $(u_1^{\max}, v_1^{\max}) = (4.10 \text{ mm}, 1166 \text{ mm/s})$ .

observed using a high-speed camera (Photron FASTCAM SA1) recording at 3000 Hz. The horizontal displacement  $u_j$  of the  $j$ th square located in the third row [highlighted by a horizontal orange line in Fig. 1(a)] is then obtained by tracking the marker positioned at its center with a digital image correlation analysis [25].

In Figs. 1(b)–1(e) we show results for two experiments in which the impactor prescribes a displacement signal to the first square characterized by  $(u_1^{\max}, v_1^{\max}) = (\max(u_1), \max(v_1)) = (3.11 \text{ mm}, 524 \text{ mm/s})$  and  $(u_1^{\max}, v_1^{\max}) = (4.10 \text{ mm}, 1166 \text{ mm/s})$  ( $v_1$  denoting the velocity of the first square), respectively. Note that the input displacement and velocity profiles [i.e.,  $u_1(t)$  and  $v_1(t)$ ] are shown in Fig. S2 of SM [23]. The evolution of the horizontal displacements  $u_j$  indicates that there is a pulse propagating through the sample that is reflected a couple of times by the boundaries before vanishing [Figs. 1(b) and 1(d)]. Moreover, by comparing the displacement  $u_j$  of all squares at different times [Figs. 1(c) and 1(e)], we find that the pulses conserve their spatial shape during propagation, suggesting that the system can support

the propagation of solitary waves. The experimental movies also reveal that the squares not only move horizontally when the pulse propagates, but also rotate (see Movies S1, S2, and S3 of SM [23]). However, the image resolution (about 20 pixels per square edge length) is not enough to monitor with sufficient accuracy their rotation. To capture the rotational waves propagating through the sample, we conduct an additional set of experiments where the camera is focused only on four squares, located at two-thirds of the sample. The results reported in Fig. S1 and Movie S3 of SM [23] clearly confirm the simultaneous propagation of translational and rotational waves in our structure.

To get a better understanding of the dynamic response of the structure, we investigate its behavior both numerically and analytically. Since our experiments indicate that, when the pulse propagates, the squares remain rigid and the deformation localizes at the hinges, we introduce a discrete model composed of periodically arranged rigid squares connected by linear springs at their vertices [see Fig. 2(a)]. More specifically, since the applied deformation is found to induce both translation and rotation of the squares [18–20], we consider two linear springs at each vertex, a compression or tension spring with stiffness  $k$  and a torsional spring with stiffness  $k_\theta$ . Moreover, since we only consider the propagation of planar waves in the  $x$  direction, guided by our experiments we assign two degrees of freedom to the  $j$ th rigid square: the displacement in the  $x$  direction  $u_j$  and the rotation  $\theta_j$  [see Fig. 2(a)]. Note that, as indicated by the blue and red arrows in Fig. 2(a), we define the positive direction of rotation alternatively for neighboring squares [i.e., if for the  $j$ th square a clockwise rotation is positive, then for the  $(j-1)$ th and  $(j+1)$ th ones counterclockwise rotation is considered as positive].

Assuming periodic boundary conditions in the  $y$  direction, it follows that the governing equations of motion for the  $j$ th square can be written as (see SM for details [23])

$$m \frac{\partial^2 u_j}{\partial t^2} = k[u_{j+1} - 2u_j + u_{j-1} - l \cos(\theta_{j+1} + \theta_0) + l \cos(\theta_{j-1} + \theta_0)] + \frac{k_\theta}{l} (\theta_{j+1} - \theta_{j-1}) \sin(\theta_j + \theta_0), \quad (1)$$

$$J \frac{\partial^2 \theta_j}{\partial t^2} = -k_\theta (\theta_{j+1} + 6\theta_j + \theta_{j-1}) - kl(u_{j+1} - u_{j-1}) \sin(\theta_j + \theta_0) + kl^2 \cos(\theta_j + \theta_0) [\sin(\theta_{j+1} + \theta_0) + \sin(\theta_{j-1} + \theta_0) - 2 \sin(\theta_j + \theta_0)] + kl^2 \sin(\theta_j + \theta_0) [\cos(\theta_{j+1} + \theta_0) + 6 \cos(\theta_j + \theta_0) + \cos(\theta_{j-1} + \theta_0) - 8 \cos(\theta_0)], \quad (2)$$

where  $m$  and  $J$  denote the mass and the moment of inertia of the squares, respectively. For the structure considered in

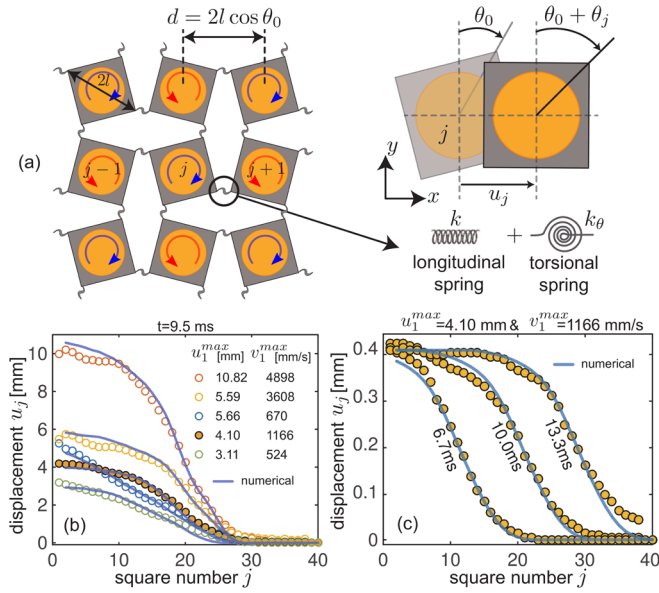


FIG. 2. (a) Schematics of the system. (b) Spatial displacement profiles at time  $t = 9.5$  ms for five different impacts characterized by different combinations of  $u_1^{\max}$  and  $v_1^{\max}$ . (c) Spatial displacement profiles at  $t = 6.7, 10$  at  $13.3$  ms for a single experiment with  $(u_1^{\max}, v_1^{\max}) = (4.10 \text{ mm}, 1166 \text{ mm/s})$ . In (b) and (c) both experimental results (markers) and numerical prediction (blue lines) are shown.

this study, we have  $m = 2.093 \text{ g}$  and  $J = 18.11 \text{ g mm}^2$ . Moreover, the stiffnesses  $k$  and  $k_\theta$  can be estimated from the experimentally measured maximal group velocity and numerically calculated stiffness under uniaxial compression, respectively (see SM for details [23]), yielding  $k = 19235 \text{ N/m}$  and  $k_\theta = 0.0427 \text{ Nm/rad}$ . Finally, we note that in this model we neglect the effect of damping, which is known to have a pronounced effect on the dynamic response of structures made of soft materials. This is because here we focus on waves propagating for a relatively short distance (before reflection at the right boundary). In this case we find that damping reduces the displacement amplitude by less than 10% and does not alter the studied nonlinear effects.

To test the relevance of our discrete model, we numerically solve Eqs. (1) and (2) using the Runge-Kutta method and compare their predictions to our experimental results. In our numerical analysis we consider a chain comprising 40 squares, apply the experimentally extracted displacement signal  $u_1(t)$  to the first square on the left [while fixing its rotation, i.e.,  $\theta_1(t) = 0$ ], and implement free-boundary conditions at the right end. In Fig. 2(b) we report numerical and experimental results at  $t = 9.5$  ms for different impact conditions, while in Fig. 2(c) we focus on an impact for which  $u_1^{\max} = 4.10 \text{ mm}$  and  $v_1^{\max} = 1166 \text{ mm/s}$  and compare the numerical predictions and experimental data at different times. Both plots show that the pulse profiles and amplitudes are well captured by the discrete model. Moreover, the numerical results in Fig. 2(c) confirm that

for certain impact conditions the pulse propagates with no apparent distortion.

While Eqs. (1) and (2) contain the full nonlinear and dispersive terms of the modeled system, a deeper insight into its dynamics can be achieved by further simplifying them to derive analytical solutions. To this end, we first introduce the normalized displacement  $U_j = u_j/2l \cos(\theta_0)$ , time  $T = t\sqrt{k/m}$ , stiffness  $K = k_\theta/kl^2$ , and inertia  $\alpha = l/(\sqrt{J/m})$  (see SM for details [23]). Second, we take the continuum limit of Eqs. (1) and (2) and retain the nonlinear terms up to second order, as well as the dominant dispersion terms, obtaining (see SM for details [23])

$$\frac{\partial^2 U}{\partial T^2} = \frac{\partial^2 U}{\partial X^2} + (1 - K) \tan(\theta_0) \frac{\partial \theta}{\partial X}, \quad (3)$$

$$\begin{aligned} \frac{\partial^2 \theta}{\partial T^2} = & \alpha^2 \left\{ [\cos(2\theta_0) - K] \frac{\partial^2 \theta}{\partial X^2} - 2 \sin(2\theta_0) \frac{\partial U}{\partial X} \right. \\ & - 4 \left[ 2K + \cos^2(\theta_0) \frac{\partial U}{\partial X} + 2 \sin^2(\theta_0) \right] \theta \\ & \left. - 4 \sin(2\theta_0) \theta^2 \right\}, \quad (4) \end{aligned}$$

where  $X = x/2l \cos(\theta_0)$ , with  $x$  denoting the coordinate along the  $x$  axis. Finally, we introduce the traveling wave coordinate  $\zeta = X - cT$ ,  $c$  being the normalized pulse velocity, so that Eqs. (3) and (4) become

$$\frac{\partial^2 U}{\partial \zeta^2} = - \frac{(1 - K) \tan(\theta_0)}{1 - c^2} \frac{\partial \theta}{\partial \zeta}, \quad (5)$$

$$\begin{aligned} \frac{\partial^2 \theta}{\partial \zeta^2} = & 2\alpha^2 \beta \sin(2\theta_0) \frac{\partial U}{\partial \zeta} + 4\alpha^2 \beta \sin(2\theta_0) \theta^2 \\ & + 4\alpha^2 \beta \left[ 2K + \cos^2(\theta_0) \frac{\partial U}{\partial \zeta} + 2 \sin^2(\theta_0) \right] \theta, \quad (6) \end{aligned}$$

where  $\beta = [\alpha^2(\cos(2\theta_0) - K) - c^2]^{-1}$ . Note that the displacement  $U(\zeta, T)$  and rotation  $\theta(\zeta, T)$  are now continuous functions of  $\zeta$  and  $T$ . By integrating Eq. (5) with respect to  $\zeta$  and assuming a zero integration constant (i.e., a wave with a finite temporal support), we obtain

$$\frac{\partial U}{\partial \zeta} = - \frac{(1 - K) \tan(\theta_0)}{(1 - c^2)} \theta, \quad (7)$$

which can then be substituted into Eq. (6) to obtain

$$\frac{\partial^2 \theta}{\partial \zeta^2} + P\theta + Q\theta^2 = 0, \quad (8)$$

where

$$P = \frac{4\alpha^2 \beta}{(1 - c^2)} [(2c^2 - 1 - K) \sin^2 \theta_0 - 2(1 - c^2)K],$$

$$Q = \frac{2\alpha^2 \beta}{(1 - c^2)} (2c^2 - 1 - K) \sin(2\theta_0).$$

Note that Eq. (8) has the form of the well-known nonlinear Klein-Gordon equation with quadratic nonlinearity [26]. When  $P < 0$  and  $Q > 0$ , analytical solutions of Eq. (8) exist in the form of a solitary wave with a stable profile,

$$\theta = A \operatorname{sech}^2 \frac{\zeta}{W}, \quad (9)$$

where  $A$  is the amplitude of the pulse and  $c$  and  $W$  are its velocity and characteristic width, which can be determined as (see SM for details [23])

$$c = \sqrt{\frac{6K + 3(1 + K)\sin^2(\theta_0) + A(1 + K)\sin(2\theta_0)}{6K + 6\sin^2(\theta_0) + 2A\sin(2\theta_0)}},$$

$$W = \frac{1}{\alpha} \sqrt{\frac{(1 - c^2)[\alpha^2(\cos(2\theta_0) - K) - c^2]}{2(1 - c^2)K + (1 - 2c^2 + K)\sin^2(\theta_0)}}. \quad (10)$$

Finally, by substituting Eq. (9) into Eq. (7), the solution for the displacement is found as

$$U = A \frac{(1 - K)W \tan(\theta_0)}{(1 - c^2)} \left(1 - \tanh \frac{\zeta}{W}\right). \quad (11)$$

Equations (9) and (11) reveal a unique feature of our system: its ability to support an elastic vector soliton. In fact, in our nonlinear system two components—one translational and one rotational—are coupled together and copropagate without distortion nor splitting. While vector solitons have been previously observed in optics [27,28], this is the first time—to the best of our knowledge—that such a phenomenon is experimentally observed in the elastic case. Finally, we note that even in the linear regime our system supports coupled translational-rotational modes (see SM for details [23]), a feature previously only observed in granular crystals [29,30].

Next, we test the validity of our analytical solution Eqs. (9)–(11) by comparing it to numerical results obtained by direct integration of the full discrete model [Eqs. (1) and (2)]. Note that in this set of simulations we assign to the first square on the left the displacement and rotation signals given by Eqs. (9) and (11), respectively, and keep free-boundary conditions at the right end. In Fig. 3(a) we focus on the structure considered in this study (for which  $\theta_0 = 25^\circ$ ,  $\alpha = 1.7$ , and  $K = 0.073$ ) and show the profiles predicted analytically and numerically for both displacement (left axis) and rotation (right axis) assuming  $A = 0.05$ . We find an excellent agreement between our analytical (lines) and numerical (markers) results. While for this set of parameters our theory predicts the propagation of a solitary wave with velocity  $c = 0.8152$  and characteristic width  $W = 5.9071$ , the numerical simulations show the propagation of a pulse that conserves its spatial shapes and is characterized by  $c \sim 0.8030$  and  $W \sim 5.8824$ . It is important to note that, as shown by Eq. (10), both the pulse width and velocity can be tuned and controlled by

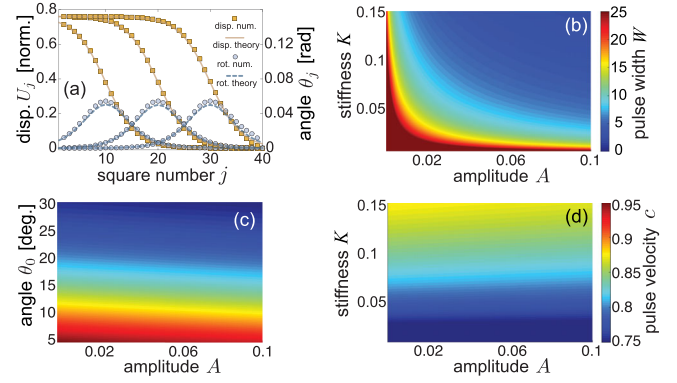


FIG. 3. (a) Comparison between analytically (lines) and numerically (markers) predicted normalized displacement and rotation profiles at  $T = 10, 20$ , and  $30$  and for  $\theta_0 = 25^\circ$ ,  $\alpha = 1.7$ ,  $K = 0.073$ . (b) Evolution of  $W$  as a function of  $A$  and  $K$  (assuming  $\theta_0 = 25^\circ$  and  $\alpha = 1.7$ ). (c) Evolution of  $c$  as a function of  $A$  and  $\theta_0$  (assuming  $K = 0.073$  and  $\alpha = 1.7$ ). (d) Evolution of  $c$  as a function of  $A$  and  $K$  (assuming  $\theta_0 = 25^\circ$  and  $\alpha = 1.7$ ).

altering either the amplitude of the wave (i.e., by changing  $A$ ) or the geometry of the structure (i.e., by changing  $\theta_0$ ,  $K$ , and  $\alpha$ ). To highlight this important point, in Figs. 3(b)–3(d) we report the evolution of  $c$  and  $W$  as a function of  $A$ ,  $K$ , and  $\theta_0$ . The contour plots indicate that  $W$  can be tuned by varying either  $A$  or  $K$ . Differently, we find that  $c$  is affected by changes in  $\theta_0$  and  $K$  (see also Fig. S5 of SM [23]). The plots also reveal another interesting feature of our system: the solitons propagate faster for smaller amplitudes.

Finally, in Fig. 4 we compare the analytical solution to our experimental results. More specifically, for each experiment we extract the maximum displacement and velocity experienced by the 1st, 2nd, 5th, 10th, 15th, and 20th squares and report them together with the analytical prediction (purple line) in the  $U^{\max}$ - $V^{\max}$  plane [where  $U^{\max} = \max(U)$  and  $V^{\max} = \max(dU/dT)$ ]. Interestingly, we find that all applied excitations result in the propagation of a soliton. If the input is close to a soliton solution, the pulse is immediately stable (i.e., even for square number  $< 5$  the experimental markers are close to the analytical curve). In contrast, if the applied impact results in a displacement signal far from that of the supported solitary wave, it takes 10–20 squares for the wave to become stable. However, it is important to note that this observation is not general and relates to the limited variety of excited displacement profiles (all of them are reasonably close to  $\tanh$ ; see Fig. S2 of SM [23]). Finally, in all experiments we find a slight displacement amplitude decrease along propagation, most probably the signature of the intrinsic material damping.

In summary, we have studied experimentally, numerically, and analytically the propagation of large-amplitude nonlinear elastic waves in a structure comprising a network of squares connected by thin and highly deformable ligaments. Our results indicate that the system supports

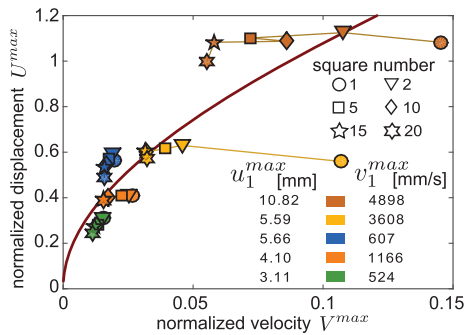


FIG. 4. Comparison between analytical solution (continuous line) and experimental results (markers). Experimental results are reported for five different impacts characterized by different combinations of  $u_1^{\max}$  and  $v_1^{\max}$ .

vector elastic solitons (i.e., stable nonlinear waves with two coupled components—one translational and one rotational), whose properties can be controlled by tuning the geometry of the structure. While in this study we focused on the propagation of planar waves in an homogeneous soft architected material, the response of such systems is very rich and there remains much to be investigated: How do nonplanar waves propagate in 2D soft architected materials? How do inhomogeneities and defects affect the propagation of the solitons? Can the system support bright or dark solitons? Can we excite topological solitons? We believe that the tools proposed in this study will help in answering all these questions and, ultimately, in designing a new class of structures and devices capable of controlling high amplitude waves and vibrations.

K. B. acknowledges support from the Materials Research Science and Engineering Center under NSF Award No. DMR-1420570. V.T. acknowledges support from ERE DGA and CNRS grants. The authors thank Professor Paulo Arratia and David Gagnon for use of and assistance with the high-speed camera, Dr. Pai Wang for fruitful discussions, and Yijie Jiang, Steven Szewczyk, Daniel Raney, and Avinash Sooriyarachchi for assistance with data collection.

- [1] R. F. Shepherd, F. Ilievski, W. Choi, S. A. Morin, A. A. Stokes, A. D. Mazzeo, X. Chen, M. Wang, and G. M. Whitesides, *Proc. Natl. Acad. Sci. U.S.A.* **108**, 20400 (2011).
- [2] D. Yang, B. Mosadegh, A. Ainla, B. Lee, F. Khashai, Z. Suo, K. Bertoldi, and G. M. Whitesides, *Adv. Mater.* **27**, 6323 (2015).
- [3] D. J. Beebe, J. S. Moore, J. M. Bauer, Q. Yu, R. H. Liu, C. Devadoss, and B.-H. Jo, *Nature (London)* **404**, 588 (2015).

- [4] S. Shan, S. H. Kang, J. R. Raney, P. Wang, L. Fang, F. Candido, J. A. Lewis, and K. Bertoldi, *Adv. Mater.* **27**, 4296 (2015).
- [5] D. Restrepo, N. D. Mankame, and P. D. Zavattieri, *Extreme Mech. Lett.* **4**, 52 (2015).
- [6] B. Florijn, C. Coulais, and M. van Hecke, *Phys. Rev. Lett.* **113**, 175503 (2014).
- [7] K. Bertoldi and M. C. Boyce, *Phys. Rev. B* **77**, 052105 (2008).
- [8] P. Wang, F. Casadei, S. Shan, J. C. Weaver, and K. Bertoldi, *Phys. Rev. Lett.* **113**, 014301 (2014).
- [9] S. Rudykh and M. C. Boyce, *Phys. Rev. Lett.* **112**, 034301 (2014).
- [10] J. Hong, *Phys. Rev. Lett.* **94**, 108001 (2005).
- [11] F. Fraternali, M. Porter, and C. Daraio, *Mech. Adv. Mater. Struct.* **17**, 1 (2009).
- [12] N. Boechler, G. Theocharis, and C. Daraio, *Nat. Mater.* **10**, 665 (2011).
- [13] T. Devaux, V. Tournat, O. Richoux, and V. Pagneux, *Phys. Rev. Lett.* **115**, 234301 (2015).
- [14] F. Li, P. Anzel, J. Yang, P. Kevrekidis, and C. Daraio, *Nat. Commun.* **5**, 5311 (2014).
- [15] A. Spadoni and C. Daraio, *Proc. Natl. Acad. Sci. U.S.A.* **107**, 7230 (2010).
- [16] V. F. Nesterenko, *J. Appl. Mech. Tech. Phys.* **24**, 733 (1984).
- [17] J. Cabaret, V. Tournat, and P. Béquin, *Phys. Rev. E* **86**, 041305 (2012).
- [18] J. Grima and K. Evans, *J. Mater. Sci. Lett.* **19**, 1563 (2000).
- [19] Y. Cho, J.-H. Shin, A. Costa, T. Kim, V. Kunin, J. Li, S. Yeon Lee, S. Yang, H. Han, I.-S. Choi, and D. Srolovitz, *Proc. Natl. Acad. Sci. U.S.A.* **111**, 17390 (2014).
- [20] S. Shan, S. Kang, Z. Zhao, L. Fang, and K. Bertoldi, *Extreme Mech. Lett.* **4**, 96 (2015).
- [21] J. A. Lewis, *Adv. Funct. Mater.* **16**, 2193 (2006).
- [22] J. R. Raney and J. A. Lewis, *MRS Bull.* **40**, 943 (2015).
- [23] See Supplemental Material at <http://link.aps.org/supplemental/10.1103/PhysRevLett.118.204102>, which includes Refs. [4, 21, 24], for a description of the experiments, details on the model, and supporting movies.
- [24] J. R. Raney, N. Nadkarni, C. Daraio, D. M. Kochmann, J. A. Lewis, and K. B. Bertoldi, *Proc. Natl. Acad. Sci. U.S.A.* **113**, 9722 (2016).
- [25] M. Senn, <https://www.mathworks.com/matlabcentral/fileexchange/50994-digital-image-correlation-and-tracking>.
- [26] T. Dauxois and M. Peyrard, *Physics of Solitons* (Cambridge University Press, Cambridge, England, 1967).
- [27] Z. Chen, M. Segev, and D. N. Christodoulides, *Rep. Prog. Phys.* **75**, 086401 (2012).
- [28] S. Manakov, *Sov. J. Exp. Theor. Phys.* **38**, 248 (1974).
- [29] F. Allein, V. Tournat, V. Gusev, and G. Theocharis, *Appl. Phys. Lett.* **108**, 161903 (2016).
- [30] A. Merkel, V. Tournat, and V. Gusev, *Phys. Rev. Lett.* **107**, 225502 (2011).